mathematics

MDPI

Article

Hybrid Statistical and Numerical Analysis in Structural Optimization of Silicon-Based RF Detector in 5G Network

Tan Yi Liang [1], Nor Farhani Zakaria [1,2,3,*], Shahrir Rizal Kasjoo [1,2], Safizan Shaari [1,2], Muammar Mohamad Isa [1], Mohd Khairuddin Md Arshad [1], Arun Kumar Singh [4] and Sharizal Ahmad Sobri [5,6]

1 Faculty of Electronic Engineering Technology, Universiti Malaysia Perlis (UniMAP), Arau 02600, Perlis, Malaysia; liangtan@studentmail.unimap.edu.my (T.Y.L.); shahrirrizal@unimap.edu.my (S.R.K.); safizan@unimap.edu.my (S.S.); muammar@unimap.edu.my (M.M.I.); mohd.khairuddin@unimap.edu.my (M.K.M.A.)
2 Micro & Nano Electronics (MiNE) Research Group, Faculty of Electronic Engineering Technology, Universiti Malaysia Perlis (UniMAP), Arau 02600, Perlis, Malaysia
3 Advanced Communication Engineering, Centre of Excellence (ACE), Universiti Malaysia Perlis (UniMAP), Kangar 01000, Perlis, Malaysia
4 Department of Electronics and Communication Engineering, Punjab Engineering College (Deemed to be University), Sector-12, Chandigarh 160012, India; arunkumar.singh@outlook.com
5 Advanced Material Research Cluster, Faculty of Bioengineering and Technology, Universiti Malaysia Kelantan, Jeli Campus, Jeli 17600, Kelantan, Malaysia; sharizal.s@umk.edu.my
6 Geopolymer and Green Technology, Centre of Excellence (CEGeoGTech), Universiti Malaysia Perlis (UniMAP), Kangar 01000, Perlis, Malaysia
* Correspondence: norfarhani@unimap.edu.my

Abstract: In this study, a hybrid statistical analysis (Taguchi method supported by analysis of variance (ANOVA) and regression analysis) and numerical analysis (utilizing a Silvaco device simulator) was implemented to optimize the structural parameters of silicon-on-insulator (SOI)-based self-switching diodes (SSDs) to achieve a high responsivity value as a radio frequency (RF) detector. Statistical calculation was applied to study the relationship between the control factors and the output performance of an RF detector in terms of the peak curvature coefficient value and its corresponding bias voltage. Subsequently, a series of numerical simulations were performed based on Taguchi's experimental design. The optimization results indicated an optimized curvature coefficient and voltage peak of 26.4260 V^{-1} and 0.05 V, respectively. The alternating current transient analysis from 3 to 10 GHz showed the highest mean current at 5 GHz and a cut-off frequency of approximately 6.50 GHz, indicating a prominent ability to function as an RF detector at 5G related frequencies.

Keywords: silicon-on-insulator (SOI); self-switching diode (SSD); curvature coefficient; Taguchi method; ANOVA; regression

Citation: Yi Liang, T.; Zakaria, N.F.; Kasjoo, S.R.; Shaari, S.; Isa, M.M.; Arshad, M.K.M.; Singh, A.K.; Sobri, S.A. Hybrid Statistical and Numerical Analysis in Structural Optimization of Silicon-Based RF Detector in 5G Network. *Mathematics* **2022**, *10*, 326. https://doi.org/10.3390/math10030326

Academic Editors: Araceli Queiruga-Dios, Maria Jesus Santos, Fatih Yilmaz, Deolinda M. L. Dias Rasteiro, Jesús Martín Vaquero and Víctor Gayoso Martínez

Received: 7 December 2021
Accepted: 17 January 2022
Published: 21 January 2022

1. Introduction

The rapid evolution of modern wireless networks and maturing 4G networks has paved the path to the new 5G communication generation, which is no longer exclusively an advancement of legacy 4G mobile networks and behaves as a system with several fresh carrier proficiencies [1]. This emerging 5G technology provides low latency and ultra-high-speed massive connectivity between devices, leading to cross-industry transformations and pervasive processing in an ecosystem where all devices are interconnected. However, it also faces various challenges [2]. To effectively employ these inclusive ideas, a range of applied sciences is required, such as heterogeneous networks, large multiple-input multiple-output, millimeter wave (mmWave) detection, device-to-device communications, software-defined networks, network function visualization, and networking slicing [1]. The motivation of this paper is in the scope of mmWave detection improvement, where a unique, low-cost radio frequency (RF) detector suitable for 5G networks is proposed,

both for signal detection and for opportunistically reusing the cellular spectrum and energy efficiency for future RF energy harvesting applications. The critical aspect of this operation is to ensure sufficient efficiency in detecting the received RF signal in the zero-bias condition to convert it into useful energy [3,4]. Zero-bias detectors in 5G networks have been reported using metal oxide semiconductor field effect transistors [5], PN junction diodes [6], and Schottky diodes. Schottky diodes have been most commonly used because of their inherently low turn-on voltages [7]. However, they require a sophisticated nanogate fabrication process that often results in parasitic effects and the coupling of a Schottky device with antennas and waveguides; moreover, the fabrication of large arrays poses additional engineering issues [8]. In addition, self-switching devices (SSDs) have received attention from researchers worldwide as they have been reported to effectively function as zero-bias RF detectors [9–11]. The rectification property of the SSD is dependent on the nonlinear IV characteristic of the device, which can be obtained by controlling the electric-field-independent zone (depletion region) of the SSD asymmetric channel. The L-shaped channel can be simply realized by electron beam lithography and chemical etching and does not involve junctions, doping, or the third gate terminal, being more adequate in terms of fabrication complexity compared to the most-used Schottky diode [12] (more details on the SSD working principle and mechanism can be found in [13]).

Several works on SSDs have focused on the detection and application in the "terahertz (THz) gap" region, the region from 0.1 THz to 10 THz on the electromagnetic spectrum where functionable detectors are scarcely reported [14]. To function in this high-frequency region, the use of high-mobility substrate materials, such as III-V materials (InGaAs, GaAs, InAs, and GaN) [10], is mandatory. Exploration of the usage of SSD in the lower 5G network region, which targets frequencies from approximately 3 to 5 GHz in the sub-6 GHz region in the worldwide communication spectrum [15], has been reported in a small number of studies using silicon as an alternative substrate [16–19], as the mobility of electrons is sufficiently high to accommodate the transition of the sinusoidal RF wave, with the advantage of a considerably lower cost compared to that of III-V materials. Optimization of the structural and material parameters of the SSD is crucial for manipulating nonlinear IV characteristics of the device, which strongly influence the rectification performance of the SSD [20]. Most optimization approaches of the SSD involve varying the channel length, L, channel width, W, and channel trench, W_t, where the depletion region is more affected to control the electron flow. Almost all reported optimization processes were performed using the trial-and-error method, where the parameters were individually varied using a range of values without any structured optimization method [21–24]. In this work, we propose the integration of a statistical analysis using the Taguchi optimization method, supported by the analysis of variance (ANOVA) and regression analysis with a numerical simulation to determine the best structural parameters of a silicon-on-insulator (SOI)-based SSD to achieve the best responsivity in the zero-bias region.

The Taguchi method has been widely used in quantitative research and reported in recent studies on experiment-based procedures to obtain an optimized result and produce high product quality by reducing the production cost using robust design experiments [13,25]. Integration of the Taguchi method with numerical analysis in simulation-based research was also reported using device simulators such as ANSYS [26,27] and ATLAS [20,28]. This shows the capability of the integration between statistical and numerical analysis to reduce the number of simulations and to obtain a prominent result with the aid of the noise ratio analysis in the Taguchi method [14]. Apart from the Taguchi, other designs of experiments (DOE) such as the central composite design and Box–Behnken design, or other quasi-random sequences can be an alternative. These alternatives may offer more precise results in trend prediction involving a higher number of runs and are more complex in design, but are not in the scope of this work. In this study, numerical simulations using the ATLAS device simulator were performed, corresponding to the DOE and analysis of the Taguchi method to obtain the highest curvature coefficient, γ, of a device that is proportional to the responsivity of the detector [28]. In addition, ANOVA and regression

analyses were performed to further analyze the sensitivity of the corresponding control factors. By integrating an organized optimization method and numerical simulation, we aimed for an optimized SOI-SSD structure with high responsivity in the 5G network region.

2. Materials and Methods

The SSD was characterized using a Silvaco ATLAS two-dimensional (2D) simulator with a top-view (TV) simulation. Figure 1a shows the geometry of a silicon-based SSD with air as the dielectric in the etched channel of the device (white area), and the cross-section of the device is shown in Figure 1b.

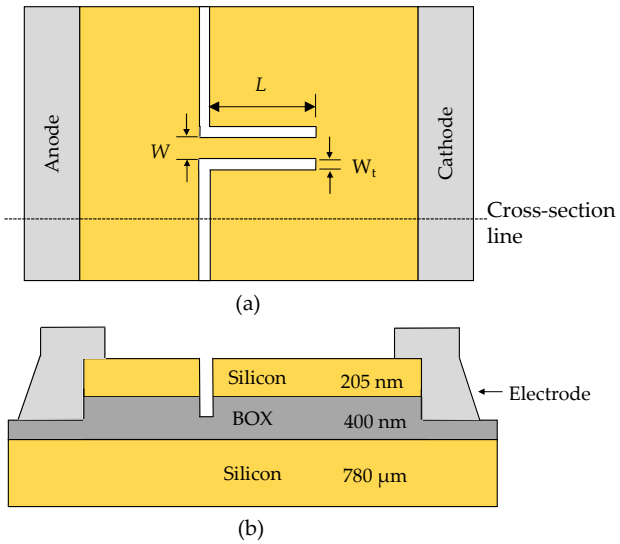

Figure 1. (**a**) Structural parameters of an SOI-based SSD, showing three main control factors: L, W, and W_t, and (**b**) the cross-section of the device.

By considering the three-dimensional (3D) nature of the diode, we assigned an approximate positive background doping of 2.45×10^{16} cm^{-3} and an interface charge density of 3.16×10^{11} cm^{-2} along the channel [16,29]. Physical models such as Klaassen's unified low-field mobility model, the Watt model, Auger recombination, and the energy balance transport model [30] were defined in the simulation to simulate the electron transport and imitate the mechanism of the real device. The materials and physical models used in the simulation were validated by comparing the electrical characteristics with those of a fabricated SOI SSD from [16], and the results were in good agreement, as shown in Figure 2.

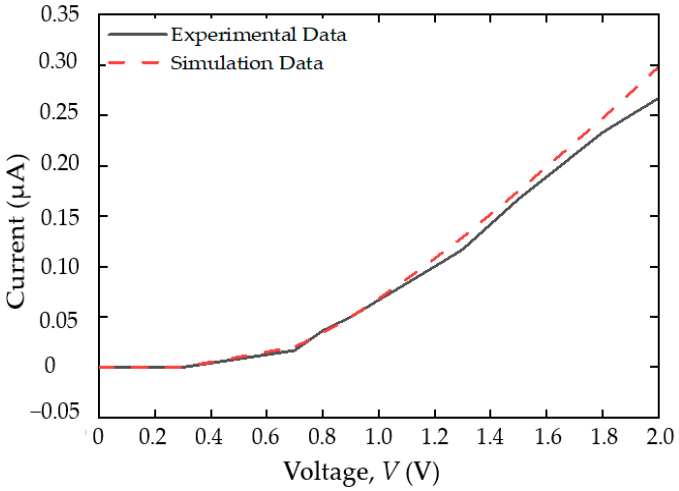

Figure 2. Comparison of IV characteristics between simulation and experimental data of Farhi et al. [16].

2.1. Determination of Control Factors and Levels for the Design of Experiment

Prior to the DOE in the Taguchi method, a series of simulations were conducted by varying the individual geometrical parameters of SSD: channel length, L, channel width, W, and trench width, W_t (refer to Figure 1a). These are the primary parameters affecting the depletion region in the SSD channel, which controls the on–off condition of the device. We have reported the performance of these individually varied parameters and their physical explanation in [19]. The control factors and their levels in this optimization work were selected based on the best electrical performance (high forward current and low leakage current) in each reported variation and are listed in Table 1.

Table 1. Control factors and their level parameters selected from analysis of individual parameters and their electrical performance.

Control Factors	Level (μm)		
	1	**2**	**3**
Channel Length, L	1.100	1.200	1.300
Channel Width, W	0.228	0.230	0.232
Trench Width, W_t	0.200	0.150	0.100

2.2. Selection of Suitable Orthogonal Array

To determine a suitable orthogonal array for the DOE, the degrees of freedom must be considered, and they are defined as the number of comparisons between the process parameters of an experiment and the levels [31]. In this study, three control factors and three levels with nine degrees of freedom were used [28]; thus, an L9 orthogonal array of Taguchi's DOE was implemented. The run number and its parameters with their corresponding level values are listed in Table 2.

Table 2. DOE using selected control factors and their level parameters for SSD optimization.

Run No.	Control Factors (Level)			Parameter Values (μm)		
	Channel Length, L	**Channel Width, W**	**Trench Width, W_t**	**Channel Length, L**	**Channel Width, W**	**Trench Width, W_t**
1	L_1	W_1	W_{t1}	1.100	0.228	0.200
2	L_1	W_2	W_{t2}	1.100	0.230	0.150
3	L_1	W_3	W_{t3}	1.100	0.232	0.100
4	L_2	W_1	W_{t3}	1.200	0.228	0.100
5	L_2	W_2	W_{t1}	1.200	0.230	0.200
6	L_2	W_3	W_{t2}	1.200	0.232	0.150
7	L_3	W_1	W_{t2}	1.300	0.228	0.150
8	L_3	W_2	W_{t3}	1.300	0.230	0.100
9	L_3	W_3	W_{t1}	1.300	0.232	0.200

2.3. Evaluation of Curvature Coefficient Peak Value and Its Corresponding Voltage

By using the structural parameters from the DOE table, the IV characteristic performance of each run was numerically simulated using the ATLAS device simulator to analyze the rectification performance. The rectification performance in a nonlinear device can be represented by the curvature coefficient, γ, which is proportional to the rectified current [14] and can be calculated as:

$$\gamma = \frac{f^{(2)}}{f^{(1)}}, \tag{1}$$

where $f^{(2)}$ and $f^{(1)}$ are the second and first derivatives, respectively, of the simulated IV characteristics. The peak value of the plotted γ versus voltage (V) and its corresponding bias voltage were recorded for further statistical analysis.

2.4. Evaluation of the Signal-to-Noise Ratio

The signal-to-noise (S/N) ratio in the Taguchi method is used to analyze the quality characteristics of each run [32]. The S/N ratio consists of three quality characteristics: nominal, lower, and higher [33]. To obtain the optimum response for this work, the S/N ratios for γ_{peak} and V_{peak} were calculated using the higher, the better (Equation (2) and the lower, the better (Equation (3) quality characteristics, respectively. The higher the γ_{peak}, the better the rectification performance in a nonlinear device, and a lower V_{peak} indicates a lower bias needed in the device to function.

$$\eta_\gamma = -10\log_{10}\frac{1}{n}\sum\frac{1}{\gamma^2}; \tag{2}$$

$$\eta_v = -10\log_{10}\frac{1}{n}\sum V^2. \tag{3}$$

3. Results and Discussion

3.1. Analysis of S/N Ratio Using Taguchi Method

The γ_{peak} and V_{peak} calculated from the simulated IV characteristics in each run and their corresponding S/N ratios from the functions of Equations (2) and (3) are listed in Table 3.

Table 3. Curvature coefficient from simulated IV characteristics and corresponding S/N ratio for each run.

Run No.	Peak of Curvature Coefficient, γ_{peak} (V^{-1})	S/N Ratio, η_γ (dB)	Corresponding Peak Voltage, V_{peak} (V)	S/N Ratio, η_v (dB)
1	23.0730	27.2621	0.1100	19.1721
2	23.3971	27.3832	0.0800	21.9382
3	18.9586	25.5561	0.0400	27.9588
4	26.0832	28.3272	0.0600	24.4370
5	24.0095	27.6077	0.1100	19.1721
6	24.2728	27.7024	0.0800	21.9382
7	27.1127	28.6634	0.1000	20.0000
8	26.4260	28.4406	0.0500	26.0206
9	24.8394	27.9028	0.1100	19.1721

The average S/N ratio from individual control factors from each run can be calculated, as shown in Table 4, by adding all similar levels for each factor or parameter according to the results in Table 3. The results are presented in Table 5.

Table 4. S/N ratio equation for each level of the control factors.

Control Factor	Level 1	Level 2	Level 3
Channel Length, L (μm)	$\eta_1 + \eta_2 + \eta_3$	$\eta_4 + \eta_5 + \eta_6$	$\eta_7 + \eta_8 + \eta_9$
Channel Width, W (μm)	$\eta_1 + \eta_4 + \eta_7$	$\eta_2 + \eta_5 + \eta_8$	$\eta_3 + \eta_6 + \eta_9$
Trench Width, W_t (μm)	$\eta_1 + \eta_5 + \eta_9$	$\eta_2 + \eta_6 + \eta_7$	$\eta_3 + \eta_4 + \eta_8$

Table 5. Calculated average S/N ratio for each level of the control factors.

Factors	Average S/N Ratio for γ_{peak} (dB)			Average S/N Ratio for V_{peak} (dB)		
	Level 1	Level 2	Level 3	Level 1	Level 2	Level 3
Channel Length, L	26.7338	27.8791	28.3356	23.0230	21.8491	21.7309
Channel Width, W	28.0842	27.8105	27.0537	21.2030	22.3770	23.0230
Trench Width, W_t	27.5909	27.9164	27.4413	19.1721	21.2921	26.1388

The overall S/N ratios for both γ_{peak} and V_{peak} were calculated using the expression:

$$\eta_{overall} = \frac{(\eta_{\gamma avg} + \eta_{vavg})}{2}. \quad (4)$$

The results are tabulated in Table 6 and plotted in Figure 3 for a better visualization of the S/N values of the levels for each control factor. As observed, the highest S/N ratio level of each control parameter can be determined and used as the optimal parameter of the SSD, as shown in Figure 4, where the L, W, and W_t are 1.30 µm, 0.23 µm, and 0.10 µm, respectively.

Table 6. Overall S/N ratio in each level of the control factors.

Factors	Level			Optimal Parameter
	1	2	3	
Channel Length, L	24.8784	24.8641	25.0333	L_3
Channel Width, W	24.6436	25.0937	25.0384	W_2
Trench Width, W_t	23.3815	24.6042	26.7901	W_{t3}

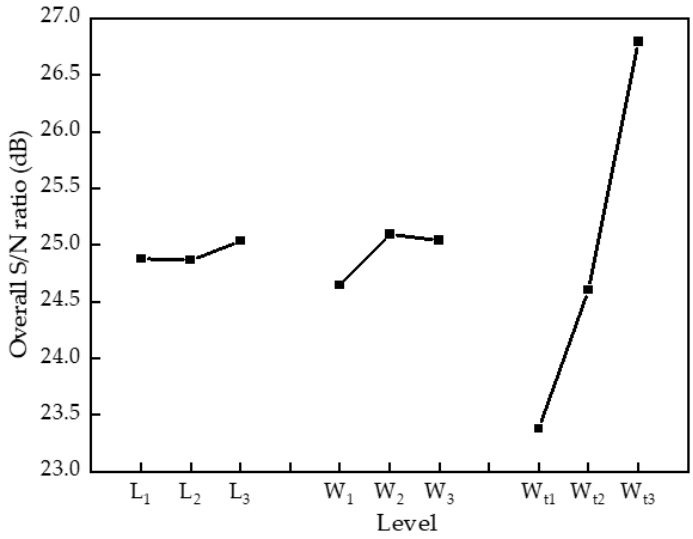

Figure 3. Overall S/N ratio for each control factor level.

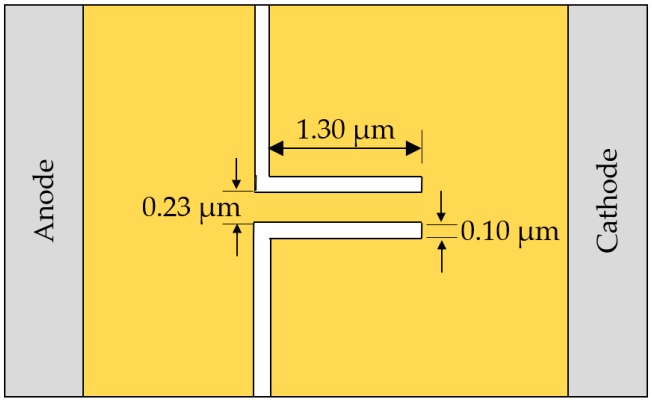

Figure 4. Optimized structure obtained from Taguchi method.

3.2. Taguchi Method with ANOVA and Regression Analysis

3.2.1. Analysis of S/N Ratio

To understand the sensitivity of the involved geometrical parameters to the RF signal response and to validate the optimized structure results obtained from the Taguchi method, ANOVA and regression analysis were conducted using Minitab statistical tool software to assist in solving the statistical and S/N ratio equations.

The S/N ratios for both γ_{peak} and V_{peak} obtained using the Minitab statistical tool were equal to those calculated using the Taguchi method in Table 3, and the average S/N ratio is shown in Table 7. The delta values in the table refer to the difference between the highest average S/N ratio and the lowest S/N ratio for each control factor and were calculated using rank values to determine the most influential control factor for both observed parameters [34,35]. From the delta values, it can be seen that the most influential factors for γ and V are L and W_t, respectively. Figures 5 and 6 show the main effect plots for γ and V, respectively. As observed, the degree of the slope in L for γ and W_t for V is the highest, indicating the presence and proportionality of the main effects [34,35].

Table 7. Response table of S/N ratio for the curvature coefficient γ and corresponding voltage V.

Levels	S/N Ratio for Curvature Coefficient, γ (dB)			S/N Ratio for Corresponding Voltage, V (dB)		
	Channel Length, L	**Channel Width, W**	**Trench Width, W_t**	**Channel Length, L**	**Channel Width, W**	**Trench Width, W_t**
1	26.7338	28.0843	27.5909	23.0230	21.2030	19.1721
2	27.8791	27.8105	27.9154	21.8491	22.3770	21.2921
3	28.3356	27.0538	27.4413	21.7309	23.0230	26.1388
Delta	1.60	1.03	0.48	1.29	1.82	6.97
Rank	1	2	3	3	2	1

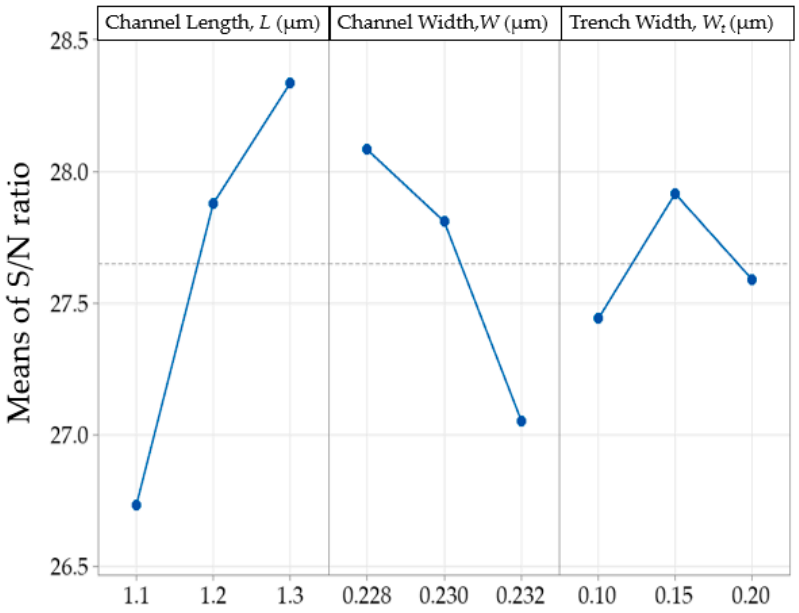

Figure 5. Plot of main effects of S/N ratio for γ.

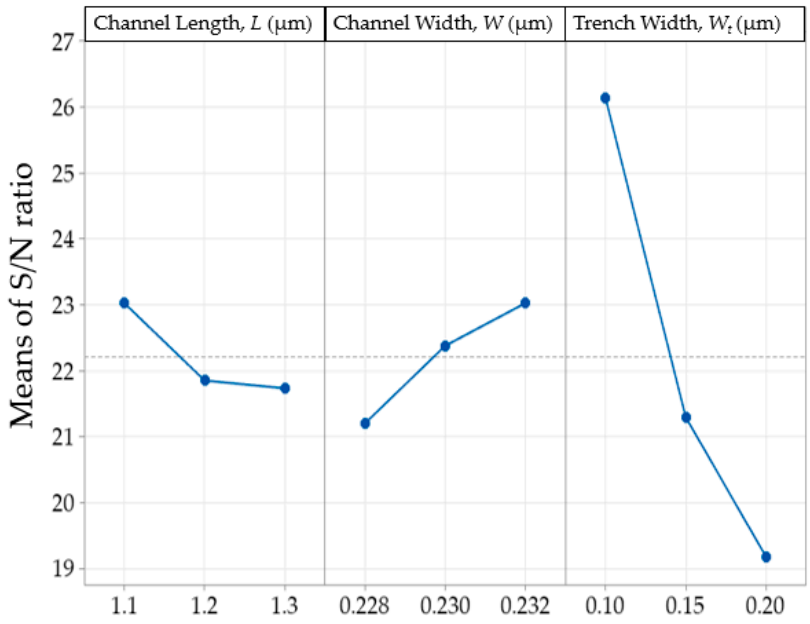

Figure 6. Plot of main effects of S/N ratio for V.

3.2.2. Analysis of Variance for S/N Ratio

To further clarify the sensitivity of geometrical parameters to the RF signal response, an ANOVA was performed for both γ and V using the equations shown in Table 8 with 95% confidence level for the p-test.

Table 8. ANOVA related equations.

Equation		Notation	
Mean Square (MS) Factor	$MS_F = \frac{SS_F}{DF_F}$	SS_F	SS Factor
		DF_F	DF Factor
MS Errors	$MS_E = \frac{SS_E}{DF_E}$	SS_E	SS Error
		DF_E	DF Error
Sum of Square (SS) Factor	$SS_F = \sum n_i(\overline{y}_{i.} - \overline{y}..)^2$	$\overline{y}_{i.}$	Mean of the observation at the ith factor level
SS Error	$SS_E = \sum_i \sum_j \left(y_{ij} - \overline{y}_{i.}\right)^2$	$\overline{y}..$	Mean of all observations
SS Total	$SS_T = \sum_i \sum_j \left(y_{ij} - \overline{y}..\right)^2$	y_{ij}	Value of the jth observation at the ith factor level
Degree of freedom (DF) Factors	$DF_F = r - 1$	n_T	Total number of observations
DF Error	$DF_E = n_T - r$	r	Number of factor levels
Total DF	$DF_T = n_T - 1$		
F-value	$F = \frac{MS_F}{MS_E}$	MS_F	MS Factor
		MS_E	MS Error
Percentage of contribution	$\% = \frac{SS_F}{SS_T}$	SS_F	SS Factor
		SS_T	SS Total

In ANOVA, the null hypothesis for the p-test is important to determine the relationship between the factors and the signal response, where the null hypothesis is rejected when there is a significant relationship between the factor and the signal response [36]. As observed in the ANOVA results of γ and V (refer to Tables 9 and 10), the null hypothesis was rejected only for W_t and V, which indicates a strong relationship between W_t and the response. However, in terms of % contribution, the % order was similar to the order of the rank from the delta results, and the % contribution for W in the γ showed a high value of 25.19% to the response. Thus, an additional regression analysis was performed to confirm the simultaneous relationship of all control factors with the results.

Table 9. ANOVA results for γ.

Source	DF	Adj SS	Adj MS	F-Value	*p*-Value	% Contribution
Channel Length, L	2	4.0859	2.0429	6.43	0.1350	60.21
Channel Width, W	2	1.7095	0.8547	2.69	0.2710	25.19
Trench Width, W_t	2	0.3540	0.1770	0.56	0.6420	5.22
Error	2	0.6359	0.3179			
Total	8	6.7852				

Table 10. ANOVA results for V.

Source	DF	Adj SS	Adj MS	F-Value	*p*-Value	% Contribution
Channel Length, L	2	3.0617	1.5309	5.49	0.1540	3.59
Channel Width, W	2	5.1080	2.5540	9.17	0.0980	5.99
Trench Width, W_t	2	76.5186	38.2593	137.30	0.0070	89.76
Error	2	0.5573	0.2787			
Total	8	85.2456				

3.2.3. Regression Analysis

The *p*-value hypothesis now involves the regression and control factors. The *p*-value in the regression analysis explains the changes in the response, where the null hypothesis of the model means that there are no significant changes to the response. As can be observed from Tables 11 and 12, the *p*-values in both regressions for γ and V reject the null hypothesis, indicating that there are variations in the parameters and responses. For the control factor parameters, L and W for γ_{peak} (refer to Table 11) and W and W_t for V_{peak} (refer to Table 12) reject the null hypothesis. These results are different from the previous analysis from ANOVA, where only W_t in the V_{peak} rejected the null hypothesis. This may occur because in the regression analysis, the coinciding factors from two sets of responses are simultaneously considered in the null hypothesis analysis, whereas in ANOVA, the individual element response is considered [37].

Table 11. Regression ANOVA for the curvature coefficient, γ.

Source	DF	Adj SS	Adj MS	F-Value	*p*-Value
Regression	3	39.1836	13.0612	8.5700	0.0200
Channel Length, L	1	27.9477	27.9477	18.3300	0.0080
Channel Width, W	1	11.2016	11.2016	7.3500	0.0420
Trench Width, W_t	1	0.0344	0.0344	0.0200	0.8870
Error	5	7.6237	1.5427		
Total	8	46.8073			

Table 12. Regression ANOVA for V.

Source	DF	Adj SS	Adj MS	F-Value	*p*-Value
Regression	3	0.005817	0.001939	69.800	0.000
Channel Length, L	1	0.000150	0.000150	5.4000	0.068
Channel Width, W	1	0.000267	0.000267	9.6000	0.027
Trench Width, W_t	1	0.005400	0.005400	194.40	0.000
Error	5	0.000139	0.000028		
Total	8	0.005956			

The relationship between the three control factors (L, W, and W_t) and their levels was studied and analyzed using linear regression. The percentages of R-sq, R-sq (adj), and R-sq (pre) values for the linear regression equations of γ and V are listed in Table 13. These values explain the variation in the response, a modification of R-sq by adjusting the number of expressions, and the precision of prediction of the model for a new observation [38]. The results indicated a good prediction percentage of 92.27% in voltage and a lower percentage value of 35.51% in curvature coefficient.

Table 13. Linear regression between control factors and response.

	Regression Equation	R-sq, %	R-sq (adj), %	R-sq (pre), %
Curvature coefficient, γ	$155.2 + 21.58L - 683W + 1.5W_t$	83.71	73.94	35.51
Voltage, V	$0.699 + 0.0500L - 3.33W + 0.6000W_t$	97.67	96.27	92.27

Thus, to determine the validity of the prediction using regression analysis, the simulated and predicted values from the simulation and regression equations were compared, as shown in Figures 7 and 8, respectively. A larger difference between the simulated and predicted results was obtained for γ compared to V, in agreement with the R-sq (pre) values in Table 13. The percentage error between the simulated and predicted results was then calculated using Equation (5):

$$\text{Percentage error} = \left| \frac{simulatedresult - predictedresult}{predictedresult} \right| \times 100\%. \quad (5)$$

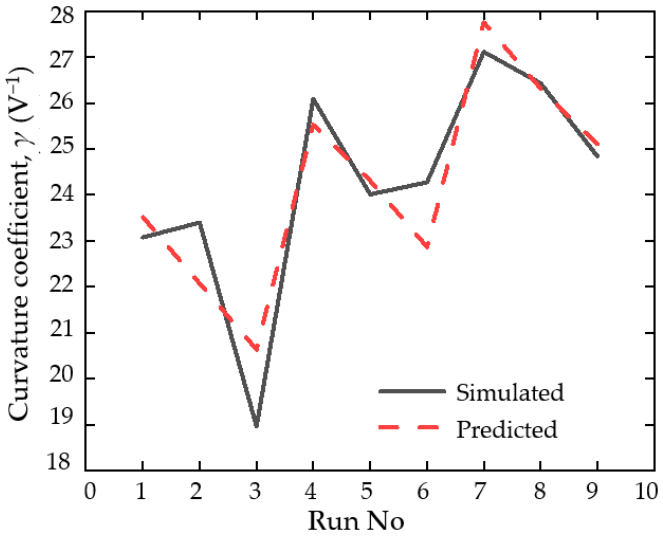

Figure 7. Comparison between predicted and simulated results for curvature coefficient peak, $\gamma_{peak.}$

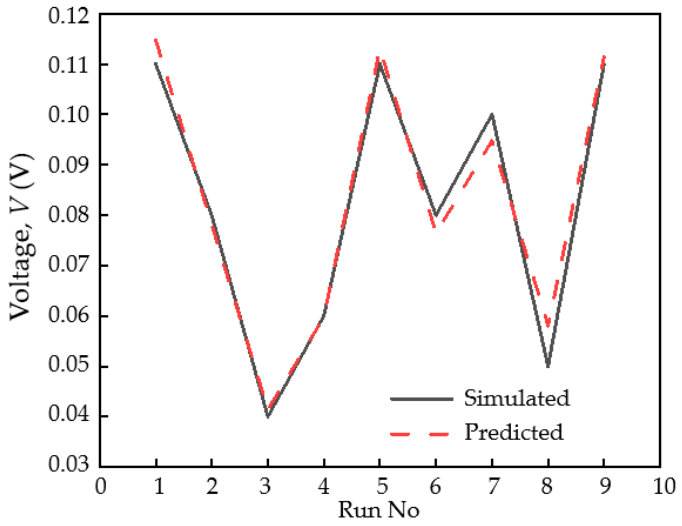

Figure 8. Comparison between predicted and simulated results for corresponding voltage, V_{peak}.

The values of the simulated and predicted results are in good agreement, with average percentage errors (from all runs) of 3.26% and 4.29% for γ and V, respectively, and are considered acceptable for a reliable statistical analysis [39].

Therefore, the response optimizer of the regression analysis was utilized in Minitab (Figure 9). From the optimizer, a high composite desirability of 0.8252 was obtained with a well-balanced rectification performance of γ and V predicted at 26.3239 V^{-1} and 0.0572 V, respectively, using the optimized structure. This balance is beneficial and achieved the objective of having high responsivity in the zero-bias region (lower than 0.3 V). The detection signal of the SOI SSD detector was then evaluated using these optimized structural parameters.

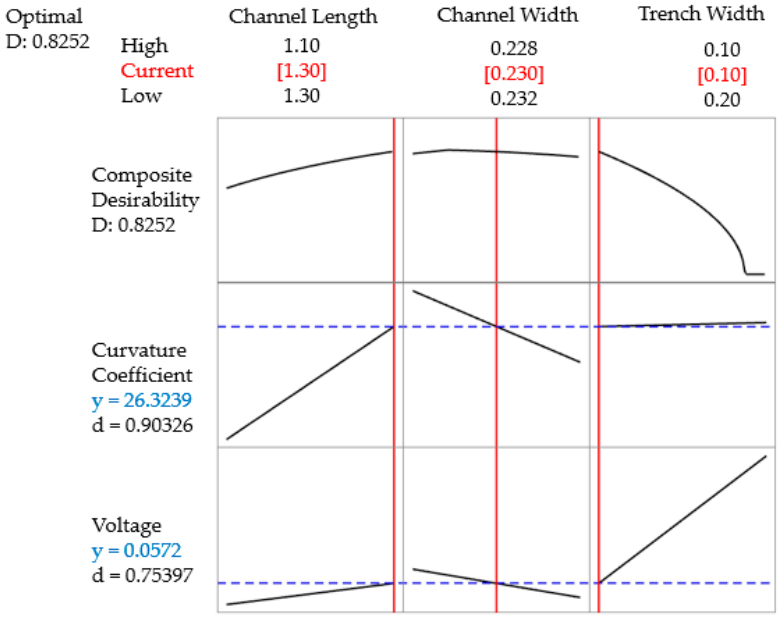

Figure 9. Response optimizer plot for regression analysis using optimized structure of SSD.

3.3. Characterization of the Optimized SSD Structure

The curvature coefficient analysis performed on the optimized structure indicated a prominent rectification performance of γ_{peak} at 26.4260 V^{-1} and V_{peak} of 0.05 V, improved from the highest reported γ value of 25.9172 V^{-1} using the trial-and-error method [19], which shows promising ability to function in zero bias (Figure 10).

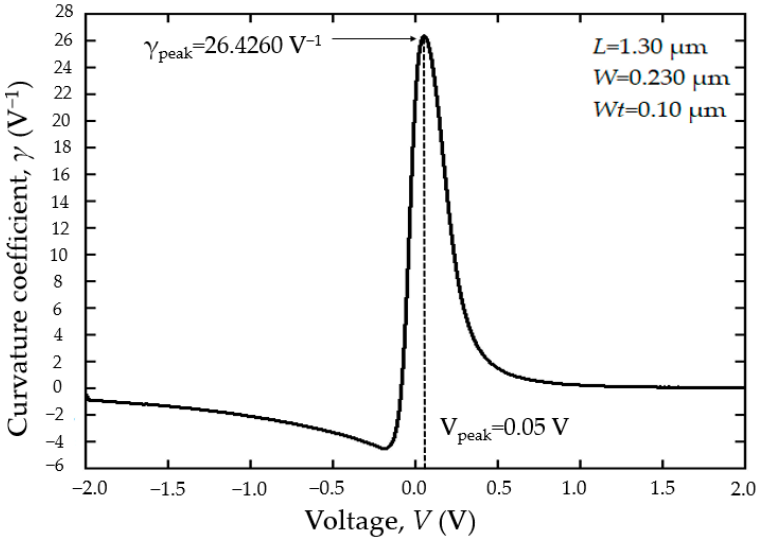

Figure 10. The curvature coefficient, γ, of the optimized SSD structure.

An alternating current (AC) transient analysis was performed on the optimized SSD structure to imitate an RF wave input of 0.30 V with a frequency ranging from 3 to 10 GHz. With 0.30 V input, the device can function in zero bias without an external power supply. In sequence, the current output for each frequency was analyzed using Equation (6) in terms of the mean current, I_{mean}, and plotted (see Figure 11) to obtain the cut-off frequency (the frequency where I_{mean} is equal to 0), which indicates no rectifying current and detection from the RF.

$$I_{mean} = \frac{1}{(t_1 - t_i)} \int_{t_i}^{t_1} f(t_1)dt - \frac{1}{(t_2 - t_1)} \int_{t_1}^{t_2} f(t_2)dt. \quad (6)$$

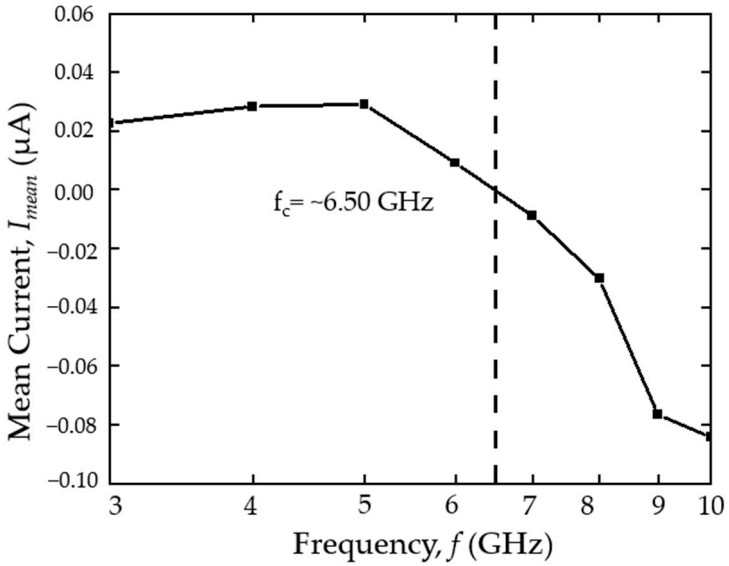

Figure 11. Cutoff frequency and the mean current values in each simulated frequency by using the optimized SSD structure.

As observed, the highest I_{mean} was obtained at 5 GHz, with a cut-off at approximately 6.50 GHz. This cutoff frequency is higher than the previously reported cutoff frequency using the SOI structure [40], which was suggested to be 4 ± 1 GHz. This indicates an improvement in the detection frequency by using an optimized structure, where an increased performance in 5G networks was achieved with the assistance of statistical optimization.

4. Conclusions

In this work, an optimized SSD structure utilized as an RF detector was analyzed by integrating statistical and numerical analyses using the Taguchi method and ATLAS device simulator, respectively. By performing numerical simulations based on Taguchi's DOE using the identified control factors and their corresponding levels, the number of significant simulation frequencies was reduced to nine runs, whereas the trial-and-error method requires a range of varied parameters in each structural parameter. Simulations were performed using the ATLAS device simulator by utilizing the physical models validated with the experimental results. The curvature coefficients, γ, from the resulting IV characteristics from each run were used for the analysis of the S/N ratios of the γ peak, and its corresponding voltage, V, was used for the overall ratio. By performing the overall calculation of the S/N ratios, the give-and-take of both γ and V was considered, where a high γ value in the lower bias voltage region was desired. The optimized structure was 0.23 μm, 1.30 μm, and 0.10 μm in channel width, channel length, and trench width, respectively.

Furthermore, the ANOVA conducted in this study provided an understanding of the sensitivity and the most affected control factors in both observed parameters of the SSD, where the γ peak value and its corresponding voltage were mostly affected by the

channel length and trench width, respectively. However, only the p-value of the trench width rejected the null hypothesis, despite the high contribution percentage of other control factors. Additional regression analysis was performed to reconfirm the simultaneous relationship of all control factors with the results, which showed the rejection of the null hypotheses in most of the parameters. From the regression analysis, it can be understood that γ was mostly affected by the channel length and width, and its corresponding voltage was dependent on the channel width and trench. The average percentage errors of the predicted and simulated S/N ratios from regression and numerical analyses in all runs were 3.26% and 4.29% for γ and V, respectively, which shows acceptable prediction using regression analysis. Analysis using the response optimizer of the regression analysis showed a favorable composite desirability of 0.8252 with well-balanced performances of γ and V predicted at 26.3239 V^{-1} and 0.0572 V, respectively, using the optimized structure.

Characterization of the optimized SSD from the Taguchi method analysis by means of ATLAS device simulator showed prominent rectification performance with a γ of 26.4260 V^{-1} at 0.05 V bias, which was improved from the highest reported γ value of 25.9172 V^{-1} using the trial-and-error method. The AC analysis of the optimized structure showed a cutoff frequency of ~6.50 GHz, which is higher than the reported cutoff of 4 ± 1 GHz, with a detection peak at 5 GHz. This shows the promising ability of the SOI SSD to function in the 5G network frequency range, which can be a good alternative for a 5G network RF detector with the advantages of fabrication simplicity and low cost.

Author Contributions: Conceptualization, N.F.Z. and S.R.K.; methodology, T.Y.L., N.F.Z. and M.M.I.; software, A.K.S.; writing—original draft preparation, T.Y.L.; writing—review and editing, N.F.Z. and M.K.M.A.; supervision, N.F.Z. and S.R.K.; project administration, S.S. and S.A.S. All authors have read and agreed to the published version of the manuscript.

Funding: This research was funded by the Ministry of Higher Education Malaysia under grant number FRGS/1/2019/STG02/UNIMAP/03/1.

Informed Consent Statement: Not applicable.

Data Availability Statement: Not applicable.

Acknowledgments: The authors would like to acknowledge support from the Fundamental Research Grant Scheme (FRGS) under grant number FRGS/1/2019/STG02/UNIMAP/03/1 from the Ministry of Higher Education Malaysia.

Conflicts of Interest: The authors declare no conflict of interest.

References

1. Pradhan, D.; Sahu, P.K.; Dash, A.; Tun, H.M. Sustainability of 5G Green Network toward D2D Communication with RF- Energy Techniques. In Proceedings of the 2021 International Conference on Intelligent Technologies (CONIT), Hubli, India, 25–27 June 2021. [CrossRef]
2. Vasjanov, A.; Barzdenas, V. A Review of Advanced CMOS RF Power Amplifier Architecture Trends for Low Power 5G Wireless Networks. *Electronics* **2018**, *7*, 271. [CrossRef]
3. Galinina, O.; Tabassum, H.; Mikhaylov, K.; Andreev, S.; Hossain, E.; Koucheryavy, Y. On feasibility of 5G-grade dedicated RF charging technology for wireless-powered wearables. *IEEE Wirel. Commun.* **2016**, *23*, 28–37. [CrossRef]
4. Shafi, M.; Zhang, J.; Tataria, H.; Molisch, A.F.; Sun, S.; Rappaport, T.S.; Tufvesson, F.; Wu, S.; Kitao, K. Microwave vs. Millimeter-Wave Propagation Channels: Key Differences and Impact on 5G Cellular Systems. *IEEE Commun. Mag.* **2018**, *56*, 14–20. [CrossRef]
5. Alaji, I.; Aouimeur, W.; Ghanem, H.; Okada, E.; Lépilliet, S.; Gloria, D.; Ducournau, G.; Gaquière, C. Design of zero bias power detectors towards power consumption optimization in 5G devices. *Microelectron. J.* **2021**, *111*, 105035. [CrossRef]
6. Alaji, I.; Aouimeur, W.; Ghanem, H.; Okada, E.; Lépilliet, S.; Gloria, D.; Ducournau, G.; Gaquière, C. Design of tunable power detector towards 5G applications. *Microw. Opt. Technol. Lett.* **2021**, *63*, 823–828. [CrossRef]
7. Eid, A.; Hester, J.; Tehrani, B.; Tentzeris, M. Flexible W-Band Rectifiers for 5G-powered IoT Autonomous Modules. In Proceedings of the 2019 IEEE International Symposium on Antennas and Propagation and USNC-URSI Radio Science Meeting, Atlanta, GA, USA, 7–12 July 2019.
8. Zakaria, N.F.; Kasjoo, S.R.; Zailan, Z.; Isa, M.M.; Arshad, M.K.M.; Taking, S. InGaAs-based planar barrier diode as microwave rectifier. *Jpn. J. Appl. Phys.* **2018**, *57*, 064101. [CrossRef]

9. Balocco, C.; Kasjoo, S.R.; Lu, X.F.; Zhang, L.Q.; Alimi, Y.; Winnerl, S.; Song, A. Room-temperature operation of a unipolar nanodiode at terahertz frequencies. *Appl. Phys. Lett.* **2011**, *98*, 223501. [CrossRef]
10. Cortes-Mestizo, I.E.; Briones, E.; Briones, J.; Droopad, R.; Perez-Caro, M.; McMurtry, S.; Hehn, M.; Montaigne, F.; Mendez-Garcia, V.H. Study of InAlAs/InGaAs self-switching diodes for energy harvesting applications. *Jpn. J. Appl. Phys.* **2015**, *55*, 014304. [CrossRef]
11. Westlund, A.; Sangaré, P.; Ducournau, G.; de la TorreI, I.; Nilsson, P.A.; Gaquière, C.; Desplanque, L.; Wallart, X.; Millithaler, J.-F.; González, T.; et al. Optimization and small-signal modeling of zero-bias InAs self-switching diode detectors. *Solid State Electron.* **2015**, *104*, 79–85. [CrossRef]
12. Zakaria, N.; Kasjoo, S.; Zailan, Z.; Isa, M.M.; Taking, S.; Arshad, M. Permittivity and temperature effects on rectification performance of self-switching diodes with different geometrical structures using two-dimensional device simulator. *Solid State Electron.* **2017**, *138*, 16–23. [CrossRef]
13. Ku, K.J.; Rao, S.S.; Chen, L. Taguchi-aided search method for design optimization of engineering systems. *Eng. Optim.* **1998**, *30*, 1–23. [CrossRef]
14. Zakaria, N.F.; Kasjoo, S.R.; Isa, M.M.; Zailan, Z.; Arshad, M.K.M.; Taking, S. Self-switching diodes as RF rectifiers: Evaluation methods and current progress. *Bull. Electr. Eng. Inform.* **2019**, *8*, 396–404. [CrossRef]
15. Ancans, G.; Bobrovs, V.; Ancans, A.; Kalibatiene, D. Spectrum Considerations for 5G Mobile Communication Systems. *Procedia Comput. Sci.* **2017**, *104*, 509–516. [CrossRef]
16. Farhi, G.; Saracco, E.; Beerens, J.; Morris, D.; Charlebois, S.; Raskin, J.-P. Electrical characteristics and simulations of self-switching-diodes in SOI technology. *Solid State Electron.* **2007**, *51*, 1245–1249. [CrossRef]
17. Aberg, M.; Saijets, J.; Pursula, E.; Prunnila, M.; Ahopelto, J. Silicon self-switching-device based logic gates operating at room temperature. In Proceedings of the Proceedings Norchip Conference 2004, Oslo, Norway, 8–9 November 2004; pp. 40–43.
18. Zailan, Z.; Kasjoo, S.R.; Zakaria, N.F.; Isa, M.M.; Arshad, M.K.M.; Taking, S. Rectification performance of self-switching diodes in silicon substrate using device simulator. In Proceedings of the 2016 3rd International Conference on Electronic Design (ICED), Phuket, Thailand, 11–12 August 2016; pp. 373–376.
19. Tan, Y.; Zakaria, N.; Kasjoo, S.; Shaari, S.; Isa, M.; Arshad, M.; Rahim, A. Numerical Simulation and Parameters Variation of Silicon Based Self-Switching Diode (SSD) and the Effect to the Physical and Electrical Properties. In Proceedings of the 2020 IEEE International RF and Microwave Conference (RFM), Kuala Lumpur, Malaysia, 14–16 December 2020.
20. Zakaria, N.F.; Kasjoo, S.R.; Zailan, Z.; Isa, M.M.; Arshad, M.K.M.; Taking, S. Rectification performance of self-switching diode in various geometries using ATLAS simulator. In Proceedings of the 2016 3rd International Conference on Electronic Design (ICED), Phuket, Thailand, 11–12 August 2016; pp. 361–364. [CrossRef]
21. IEEE. Nanotechnology Council and Institute of Electrical and Electronics Engineers. In Proceedings of the 2018 IEEE 13th Nanotechnology Materials and Devices Conference (NMDC), Portland, OR, USA, 14–17 October 2018.
22. Zailan, Z.; Zakaria, N.F.; Isa, M.M.; Taking, S.; Arshad, M.K.M.; Kasjoo, S.R. Characterization of self-switching diodes as microwave rectifiers using ATLAS simulator. In Proceedings of the 2016 5th International Symposium on Next-Generation Electronics (ISNE), Hsinchu, Taiwan, 4–6 May 2016.
23. Mateos, J.; Song, A.M.; Vasallo, B.G.; Pardo, D.; Gonzalez, T. THz operation of self-switching nano-diodes and nano-transistors. In *Nanotechnology II*; International Society for Optics and Photonics: Bellingham, WA, USA, 2005; Volume 5838, pp. 145–153.
24. Kimura, Y.; Kiso, T.; Higaki, T.; Sun, Y.; Maemoto, T.; Sasa, S.; Inoue, M.Y. Rectification effects in ZnO-based transparent self-switching nano-diodes. In Proceedings of the 2012 IEEE International Meeting for Future of Electron Devices, Kansai, Suita, Japan, 9 May 2012.
25. Stephanie, F.; Mike, O.; Ben, T.; John, Z. Design of experiments via taguchi methods: Orthogonal arrays—ControlsWiki. In *The Michigan Chemical Process Dynamics and Controls Open Text Book*; 2006; pp. 1–11. Available online: https://controls.engin.umich.edu/wiki/index.php/Design_of_experiments_via_taguchi_methods:_orthogonal_arrays (accessed on 29 November 2021).
26. Liu, S.-J.; Lin, C.-H.; Wu, Y.-C. Minimizing the sinkmarks in injection-molded thermoplastics. *Adv. Polym. Technol.* **2001**, *20*, 202–215. [CrossRef]
27. Fei, N.C.; Mehat, N.M.; Kamaruddin, S. Practical Applications of Taguchi Method for Optimization of Processing Parameters for Plastic Injection Moulding: A Retrospective Review. *ISRN Ind. Eng.* **2013**, *2013*, 462174. [CrossRef]
28. Zakaria, N.F.; Kasjoo, S.R.; Isa, M.M.; Zailan, Z.; Mokhar, M.B.M.; Juhari, N. Application of Taguchi method in optimization of structural parameters in self-switching diode to improve the rectification performance. In Proceedings of the 2nd International Conference on Applied Photonics and Electronics 2019 (Incape 2019), Putrajaya, Malaysia, 22 August 2019; AIP Publishing: Putrajaya, Malaysia, 2020; Volume 2203, p. 020047.
29. Farhi, G.; Morris, D.; Charlebois, S.; Raskin, J.-P. The impact of etched trenches geometry and dielectric material on the electrical behaviour of silicon-on-insulator self-switching diodes. *Nanotechnology* **2011**, *22*, 435203. [CrossRef]
30. ATLAS User's Manual. *Device Simulation Software*; Silvaco Inc.: Santa Clara, CA, USA, 1998; Volume II, pp. 567–1000.
31. Nalbant, M.; Gökkaya, H.; Sur, G. Application of Taguchi method in the optimization of cutting parameters for surface roughness in turning. *Mater. Des.* **2007**, *28*, 1379–1385. [CrossRef]
32. Sorgdrager, A.; Wang, R.-J.; Grobler, A. Taguchi Method in Electrical Machine Design. *SAIEE Afr. Res. J.* **2017**, *108*, 150–164. [CrossRef]

33. Yang, W.; Tarng, Y. Design optimization of cutting parameters for turning operations based on the Taguchi method. *J. Mater. Process. Technol.* **1998**, *84*, 122–129. [CrossRef]
34. Ishrat, S.I.; Khan, Z.A.; Siddiquee, A.N.; Badruddin, I.A.; AlGahtani, A.; Javaid, S.; Gupta, R. Optimising Parameters for Expanded Polystyrene Based Pod Production Using Taguchi Method. *Materials* **2019**, *7*, 847. [CrossRef]
35. Gaaz, T.S.; Sulong, A.B.; Kadhum, A.A.H.; Nassir, M.H.; Al-Amiery, A.A. Optimizing Injection Molding Parameters of Different Halloysites Type-Reinforced Thermoplastic Polyurethane Nanocomposites via Taguchi Complemented with ANOVA. *Materials* **2016**, *9*, 947. [CrossRef]
36. Qidwai, M.O.; Badruddin, I.A.; Khan, N.Z.; Khan, M.A.; Alshahrani, S. Optimization of Microjet Location Using Surrogate Model Coupled with Particle Swarm Optimization Algorithm. *Materials* **2021**, *9*, 2167. [CrossRef]
37. Zerti, O.; Yallese, M.A.; Khettabi, R.; Chaoui, K.; Mabrouki, T. Design optimization for minimum technological parameters when dry turning of AISI D3 steel using Taguchi method. *Int. J. Adv. Manuf. Technol.* **2017**, *89*, 1915–1934. [CrossRef]
38. Mohsin, I.; He, K.; Li, Z.; Zhang, F.; Du, R. Optimization of the Polishing Efficiency and Torque by Using Taguchi Method and ANOVA in Robotic Polishing. *Appl. Sci.* **2020**, *10*, 824. [CrossRef]
39. Ozcelik, B. Optimization of injection parameters for mechanical properties of specimens with weld line of polypropylene using Taguchi method. *Int. Commun. Heat Mass Transf.* **2011**, *38*, 1067–1072. [CrossRef]
40. Aberg, M.; Saijets, J. DC and AC characteristics and modeling of Si SSD-nano devices. In Proceedings of the 2005 European Conference on Circuit Theory and Design, Cork, Ireland, 2 September 2005.